Chemical Science

ROYAL SOCIETY OF CHEMISTRY

EDGE ARTICLE

View Article Online
View Journal | View Issue

Cite this: *Chem. Sci.*, 2025, **16**, 15129

All publication charges for this article have been paid for by the Royal Society of Chemistry

Uncovering intramolecular singlet fission at the root of the dual fluorescence of 1,4-bis(*p*-nitro-β-styryl)benzene in solution‡

Letizia Mencaroni,§[a] Alexandr Zaykov, §*[b] Benedetta Carlotti,[a] Fausto Elisei,[a] Guillaume Bastien,[b] Raimondo Germani,[a] Zdeněk Havlas,[b] Anna Spalletti *[a] and Josef Michl †[bc]

The exploration of singlet fission (SF) promises a pathway to many leaps forward including more efficient solar energy extraction and, more recently, organic-based quantum computing. Our study, through a joint experimental and computational approach, revolves around 1,4-bis(*p*-nitro-β-styryl)benzene (**1**) as the smallest molecule where the intramolecular transformation of the initially allowed 1^1Bu singlet state to the 2^1Ag excited state stops being ordinary internal conversion and becomes the first half of the SF process. Herein, we experimentally observe explicit breaking of the Kasha rule. Using femtosecond broadband fluorescence upconversion, we measure a dual fluorescence of **1** in solution from its two lowest singlet excited states of different symmetry. Femtosecond transient absorption (TA) and fluorescence upconversion spectroscopy of **1** in toluene reveal ultrafast (17 ± 5 ps), almost quantitative interconversion between 1^1B and 2^1A states. A sensitization bracketing experiment with ns-TA is used to analyze the T_1 state of **1**. Employing high-level *ab initio* extended multi-configuration quasi-degenerate 2nd-order perturbation theory (XMCQDPT2) calculations, we accurately model ground- and excited-state potential energy surfaces. 1^1B states are predominantly described by ordinary HOMO–LUMO excitation. 2^1A states can be projected in localized frontier molecular orbitals as an intramolecular strongly coupled triplet biexciton [$^1(T_1T_1)$] with the inclusion of intramolecular charge-transfer states. Moreover, the experimental resemblance of 2^1A and T_1 absorption is elucidated. The fluorescence temperature-dependence experiment further corroborates the XMCQDPT2 model accurate prediction of the 1^1B and 2^1A low barrier of crossing (*ca.* 600 cm^{-1}). The concentration-dependent experiment shows a dramatic increase in triplet yield: up to 200% yield is obtained by ns-TA quantitative measurements. All the obtained results suggest the occurrence of an SF mechanism for the triplet production: intramolecular $^1(T_1T_1)$ formation followed by intermolecular triplet separation aided by entropy and spatial separation.

Received 19th May 2025
Accepted 14th July 2025

DOI: 10.1039/d5sc03612g

rsc.li/chemical-science

Introduction

Singlet fission (SF) is a photophysical process in which a singlet exciton forms a singlet biexciton and then splits into two independent triplet excitons.[1–3] The process is spin-allowed and can occur at sub-picosecond times. It is of considerable interest in its own right but might also become important practically since it offers an inexpensive opportunity to overcome the Shockley–Queisser limit[4] for the energy efficiency of single-junction solar cells[5–8] or to further the boundaries of quantum computing.[9,10]

In intermolecular SF, the two triplet excitons are located on two different molecules and their ultimate independence results from loss of all spin coherence after diffusion of the triplet excitons far apart, by energy transfer in a solid or by Brownian motion in a solution. In intramolecular SF, the two triplet excitation sites are located on the same molecule and the completion of the SF process is typically harder to achieve. In a small molecule, a separation of the two strongly coupled triplet excitations in a neat solid or in solution requires a transfer of one of them to another molecule upon contact without simultaneous decay of the other. This would likely be

[a]*Department of Chemistry, Biology and Biotechnology, University of Perugia, Via dell' Elce di Sotto, 8, 06123 Perugia PG, Italy. E-mail: anna.spalletti@unipg.it*

[b]*Institute of Organic Chemistry and Biochemistry of the Czech Academy of Sciences, Prague 6 160 00, Czech Republic. E-mail: alexandr.zaykov@uochb.cas.cz*

[c]*Department of Chemistry, University of Colorado Boulder, Cristol Chemistry and Biochemistry, Boulder, CO 80309, USA*

‡ Electronic supplementary information (ESI) available: Methods, synthesis, further results of calculations, sensitization experiments, fs-TA, concentration effects, triplet quantum yield evaluation, temperature effect on fluorescence, and optimized geometries. See DOI: https://doi.org/10.1039/d5sc03612g

§ These authors contributed equally as first authors.

† Josef Michl passed away on May 13th 2024.

very endothermic, and it has received limited attention. If anything, one would expect an ordinary singlet–singlet transfer of all the excitation energy, *i.e.*, simultaneous loss of both strongly coupled triplet excitations. In a large molecule, *e.g.*, a conjugated polymer, the two triplet excitations may move sufficiently far apart to interact only weakly and to become independent while staying on the same molecule, perhaps a chain or a dendrimer. Then, a sequential transfer of two triplet excitations would be quite plausible.

We have become interested in the development of molecular photophysical properties from a limit in which the molecule is small and the two triplets interact strongly to a limit in which it is large and the triplets interact hardly at all. For instance, in a conjugated polyene, both singlet and triplet self-trapped excitons stretch over several C=C double bonds. In the smallest members of the series, such as s-*trans*-1,3-butadiene, two triplet excitations cannot move apart and are obliged to interact strongly. Their singlet coupled combination represents a reasonable description of the strongly stabilized 2^1A_g molecular state, and their triplet and quintet coupling produces states at much higher energies.[11] The interaction between the two triplets is so strong that any attempt to transfer only one of the triplet excitations to another molecule appear hopeless. The 2^1A_g excited state is like any other and if intermolecular energy transfer were to occur, all its excitation energy would be available for the purpose. Intramolecular transformation of an initial allowed 1^1B_u singlet excited state to the 2^1A_g excited state is in this case usually viewed as ordinary internal conversion.[12]

Long-chain polyacetylene is an example of the other limit, in which two localized triplet excitations can be located very far apart, such that their interaction is negligible. Here, it would be natural to view their formation from an initial singlet excitation followed by spatial separation as a case of intramolecular SF. The singlet, triplet, and quintet sublevels resulting from their interaction would be nearly exactly degenerate. The triplet–triplet absorption spectrum and the bleach in the ground state absorption spectrum would be expected to look identical to those of a single triplet exciton on the same chain, but twice as intense. The transfer of one of the triplet excitations to another molecule without a loss of the other triplet excitation should proceed without complications.

How long does a conjugated polymer need to be before its behavior approaches the infinite limit? When should one abandon the language of internal conversion and start talking about intramolecular SF? From a practical perspective, when will it be reasonable to expect an easy intermolecular transfer of one of the triplet excitations without affecting the other? This will necessarily depend on the chemical structure chosen and the transition will not be sharp. Nevertheless, even qualitative information would be of interest.

For our study, we have chosen the doubly terminally *p*-nitro substituted *p*-distyrylbenzene **1** that may exist in solution as a mixture of two different conformers **1a** and **1s**, originating from the rotation around the quasi-single bond between the central phenylene and the double bond (Fig. 1). The poly(-phenylenevinylene) series is one of the workhorses among conjugated polymers,[13–15] which sparked considerable interest

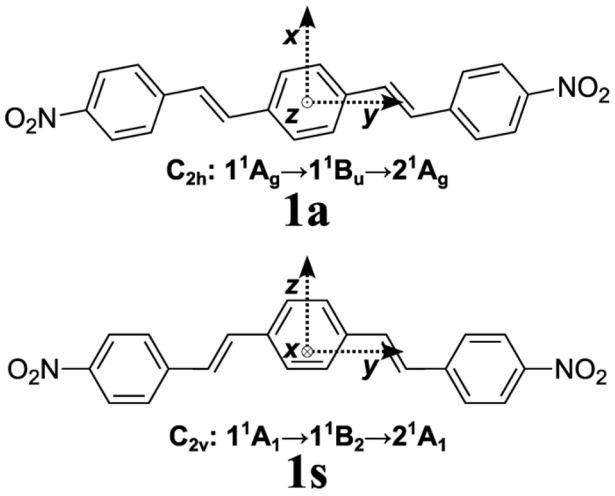

Fig. 1 Molecular structures of s-*anti* and s-*syn* conformers, **1a** (C_{2h}) and **1s** (C_{2v}), with molecular axes and irreducible representations of the ground state and two lowest singlet excited states.

in the sector of organic electronics.[16–18] In the whole series, we would expect the analogs of the 1^1B_u and 2^1A_g excited singlet states of all-s-*trans* conformers of all-*trans* polyenes to be the lowest allowed and lowest forbidden excited state, respectively. The strongly allowed transition from the ground to the 1^1B_u state may well completely bury the transition to the 2^1A_g state in the absorption spectrum and make it hard to observe.[19,20]

In a previous study (PCCP 2015),[21] we noticed how the introduction of the two nitro groups in compound **1** gives an interesting push–pull character to this quadrupolar structure introducing intramolecular charge transfer states. Virtual intramolecular charge transfer states are well known in the literature to aid intramolecular SF.[2,22–24] The experimental study was carried out by employing stationary and time-resolved spectroscopies with nanosecond (ns) and femtosecond (fs) resolution in a joint effort with extended multi-configuration quasi-degenerate perturbation theory to the second order[25–30] (XMCQDPT2) calculations. We assign the analogs of the polyene singlet 2^1A_g and 1^1B_u and 2^1A_1 and 1^1B_2 states as S_1 and S_2 for the s-*anti* and s-*syn* conformer, respectively (Fig. 1).[21] We calculate the s-*syn* (**1s**) and s-*anti* (**1a**) conformers of **1** to have nearly equal abundance in solution, and their presently relevant properties should be essentially identical. In the interpretation of the experiments, we treat their mixture as a single compound. We thus omit the symmetry-related subscripts (1,2/g,u) of the irreducible representations unless it specifies either conformer.

Results

Steady-state absorption and emission

Unless specified otherwise, all spectra were measured at room temperature in toluene at 2×10^{-5} M concentration. There were no indications of solute aggregation in any of the measurements. The experimental results are shown in Fig. 2, along with a bar diagram showing vertical absorption and fluorescence

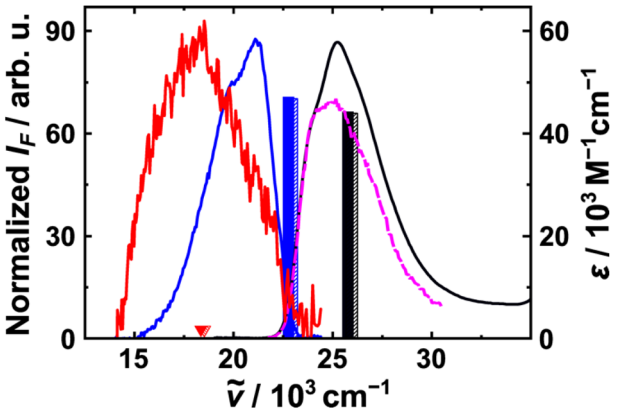

Fig. 2 Spectra of 2×10^{-5} M **1** in toluene at room temperature. Ground state absorption (black); fluorescence excitation (identical at $\tilde{\nu}_{em}$ = 21 050 cm^{-1} and 18 180 cm^{-1}) normalized to the absorption peak onset (dashed, violet); dual fluorescence from 1^1B (blue) and 2^1A (red). XMCQDPT2/ANO-L-VTZP vertical transition energies (full bars, **1a**, and hatched bars, **1s**) at optimal initial state geometries with oscillator strengths in parentheses: red: $2^1A \rightarrow 1^1A$ (0); black: $1^1A \rightarrow 1^1B$ (**1a** 1.85, **1s** 1.84); blue: $1^1B \rightarrow 1^1A$ (**1a** 1.97, **1s** 1.95).

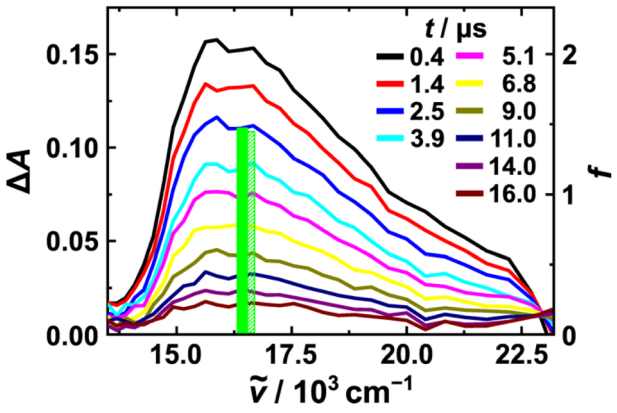

Fig. 3 Room temperature T_1 (1^3B) ns transient absorption spectra of **1** in toluene (2×10^{-5} M) and XMCQDPT2/ANO-L-VTZP vertical transition energies (full bars, **1a**, and hatched bars, **1s**) at optimal initial state geometries with oscillator strength *f* in parentheses: green: $1^3B \rightarrow 2^3A$ (**1a** 1.73, **1s** 1.69).

transition energies and respective oscillator strengths calculated using eqn (S3)‡ at XMCQDPT2/TZ level of theory (see below). The evidence of dual emission (blue and red lines), suggested in another work by a temperature effect on the fluorescence spectrum,[21] is further proven by up-conversion measurements (see below).

The fluorescence excitation spectra are independent of the monitoring wavelength. The total fluorescence quantum yield (Φ_F) is ~0.01. However, it is notable that the fluorescence excitation and absorption spectra do not agree (black and violet lines, Fig. 2). Based on the chosen normalization, the spectra agree up until the first peak of vibronic progression and lose the agreement beyond (dashed violet line).

Transient absorption in ns regime (ns-TA)

A transient appeared upon direct excitation of a 2×10^{-5} M toluene solution of **1** at $\tilde{\nu}_{exc} \cong 28\,100$ cm^{-1} with an absorption peak of $\tilde{\nu}_{Tmax} \cong 15\,600$ cm^{-1} (Fig. 3). The obtained transient spectrum was identical to the one previously recorded upon sensitization with high energy triplet donors.[21] Due to the strong oxygen effect on its lifetime, it is assigned to the lowest triplet state of **1** (1^3B).

A triplet quantum yield $\Phi_T = (0.37 \pm 0.06)$ and lifetime of 7.4 µs in deaerated toluene were already reported[21] and obtained by calibration of the optical setup to evaluate $\Phi_T \times \varepsilon_T$. Sensitization experiments provided an estimate for the triplet extinction coefficient ($\varepsilon_T = 24\,400$ M^{-1} cm^{-1}).

Additionally, ns laser flash photolysis was employed to experimentally address the triplet energy of **1** in deaerated toluene solutions. From the analysis of the kinetic quenching constant values obtained through the bracketing method (Table S9‡), **1** as a triplet donor is barely quenched by anthracene, *i.e.*, with a quenching rate constant of 1.2×10^8 $M^{-1}s^{-1}$, but efficiently by [6,6]-phenyl-C_{61}-butyric acid methyl ester.[24,31] The triplet energy of **1** was thus estimated through the Sandros equation (see the ESI,‡ Section 4, page 20)[32] to be *ca.* 1.7 eV. Being the experimentally evaluated S_1 energy of *ca.* 3.2 eV and the theoretically calculated of 3.05 eV (see below), a slightly activated SF is expected based solely on the energetic requirements.[1]

Fluorescence upconversion (FUC) and transient absorption in fs regime (fs-TA)

The fs-TA spectra for **1** in toluene evolve in time from the singlet excited state absorption peaked at ~13 000 cm^{-1} to a final triplet absorption spectrum centered at ~16 000 cm^{-1} (Fig. 4, left). On the other hand, fluorescence upconversion measurement showed that at most emission wavelengths the fluorescence decay is biexponential if initial ultrafast (~1 ps) spectral changes are ignored (Fig. 4, right). The obtained time-resolved emission spectra show an apparent red-shift and intensity reduction in time – from an intense band peaked at ~22 000 cm^{-1} right after photoexcitation to a final weak and broad spectrum centered at ~18 000 cm^{-1}. The time resolved fluorescence spectra and biexponential kinetics point to a dual fluorescence behavior of compound **1** and suggest emission from two distinct excited states.

Due to the weakness of the emission, the lifetimes τ in Table 1 were obtained by simultaneous global fitting of both time-resolved FUC and fs-TA measurements.[33] The decay constants of the two observed very short-lived species in fs-TA reflect solvation dynamics in toluene ($\tau_1 \cong 0.3$ ps; $\tau_2 = 1.2$–1.5 ps),[34] which is far beyond the temporal resolution of the ultrafast spectroscopic set-ups (black curves, Fig. 4B and E). The model assumes 1^1B to be solely responsible for (i) the TA at ~13 600 cm^{-1}; and (ii) the higher energy emission at ~21 100 cm^{-1} (blue curves, Fig. 4B–F as well as Fig. 2). 1^1B parallel non-radiative decay to 2^1A with $\tau_{dec}(1^1B) = (17 \pm 5)$ ps is responsible for the rise of 2^1A absorption (red curves, Fig. 4B and C) with $\tau_{rise}(2^1A) = (16.9 \pm 0.2)$ ps. The formed 2^1A is in turn responsible for the lower energy emission at ~18 000 cm^{-1} (red

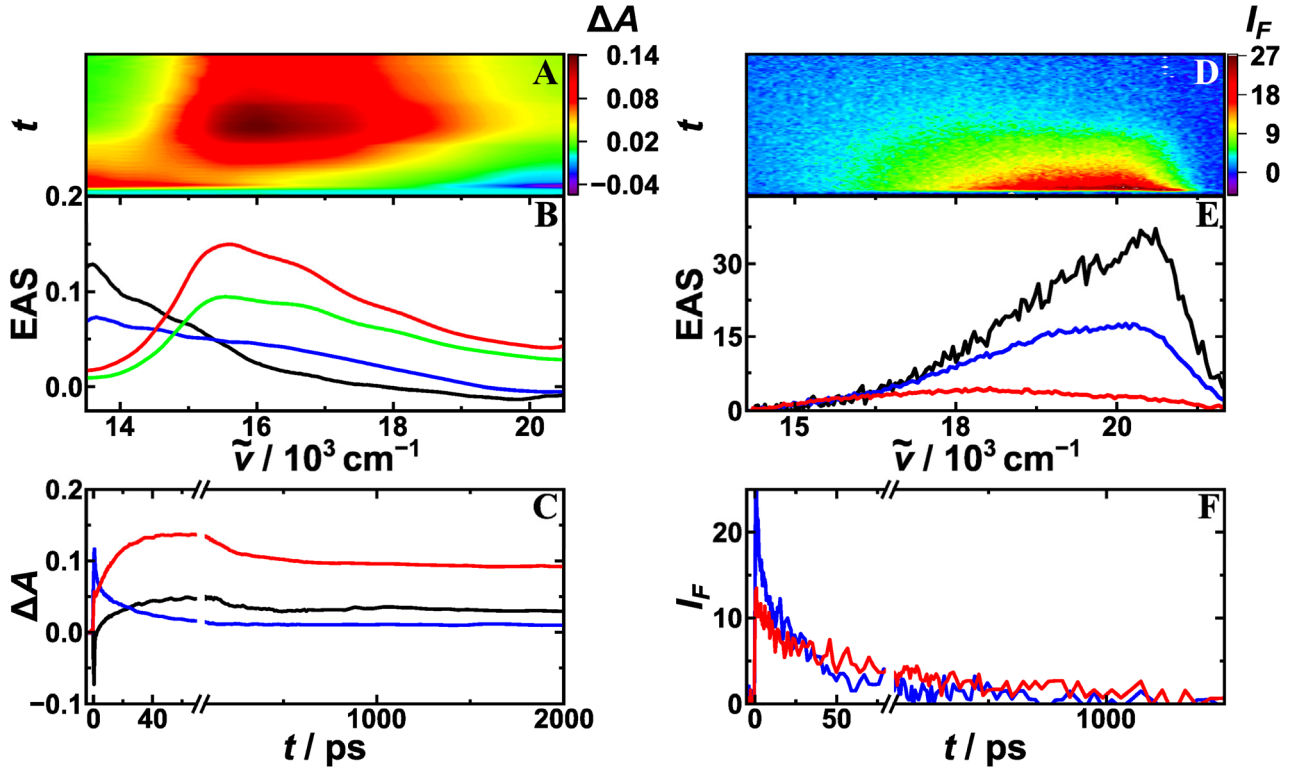

Fig. 4 Fs transient absorption (left) and fluorescence upconversion (right) of **1** in toluene at room temperature ($\tilde{\nu}_{exc}$ = 25 000 cm^{-1}). Experimental 3D data matrices for transient absorption (A) and upconversion (D). Evolution-associated spectra (EAS) obtained by global analysis of fs transient absorption (B) and upconversion (E). Transients: 1^1B ($\tau = 1.0 \pm 0.7$ ps, black), 1^1B *solv.* ($\tau = 17 \pm 5$ ps, blue), 2^1A ($\tau = 280 \pm 140$ ps, red) and 1^3B (τ = Inf, green). Representative kinetics of fs transient absorption (C) recorded at $\tilde{\nu}$ = 20 600 cm^{-1} (black); 13 600 cm^{-1} (blue); 15 600 cm^{-1} (red); and fluorescence upconversion (F) obtained at $\tilde{\nu}$ = 21 500 cm^{-1} (blue); and 18 200 cm^{-1} (red). Fluorescence intensity (I_F) and time (t) in procedure defined units, unless specified.

Table 1 Transient spectroscopy of **1** from simultaneous global analysis of fs transient absorption (ABS) and fluorescence upconversion (FUC)[a]

Trans.[b]	ABS[c] $\tilde{\nu}_{max}$ (cm^{-1})	FUC[d] $\tilde{\nu}_{max}$ (cm^{-1})	τ_{rise}[e]/ps	τ_{dec}/ps[f]
1^1B solv.	13 500	21 700		1.0 ± 0.7
1^1B	13 600	21 100		17 ± 5
2^1A	15 600	18 000	16.9 ± 0.2[e]	280 ± 140
1^3B	15 600	—		≫3.2 × 10^3

[a] 2 × 10^{-5} M in toluene, $\tilde{\nu}_{exc}$ = 25 000 cm^{-1}. [b] Transients from Fig. 3 and 4; assignment in parentheses. [c] Transient absorption peak. [d] Fluorescence peak. [e] From fitting the single-wavenumber kinetics at 15 600 cm^{-1}. [f] From global fitting.

curves, Fig. 4E and F as well as Fig. 2). Additionally, their radiative decay to the ground state is responsible for the reduction of the ground state bleach. Time dependence of the populations of the 1^1B and 2^1A states is summarized in Fig. S13.‡

The final state, generated by the decay of 2^1A with $\tau_{dec}(2^1\text{A}) = (280 \pm 140)$ ps, is only observed through fs-TA (green curve, Fig. 4B). Based on its similarity to the ns-TA spectrum (Fig. 3), it was assigned as the lowest triplet state 1^3B. Its long lifetime $\tau_{dec}(1^3\text{B})$, outside of the 3.2 ns temporal window, further supports this assignment. The absorption spectra of 2^1A and 1^3B are identical apart from the absorption coefficient of the former being ~1.5 times higher.

Fluorescence quantum yields $\Phi_F(1^1\text{B})$ and $\Phi_F(2^1\text{A})$ are derived from the experimental Φ_F and the pre-exponential factors of the biexponential decay, respectively: $\Phi_F(1^1\text{B}) \cong 0.009$ and $\Phi_F(2^1\text{A}) \cong 0.001$. The τ_{dec} and τ_{rise} constants obtained by global fitting are collected in Table 1.

Solvent polarity and temperature effects

Solvent polarity dependence on the fs-TA was gauged using toluene (ε = 2.38) and anisole (ε = 4.33) mixtures (Fig. S14 and Table S10‡). The ICT state becomes an intermediate transient species between the single-excited 1^1B species and the double triplet ^{1}A state with a slight increase in solvent polarity in toluene/anisole 70 : 30 or toluene/anisole 1 : 1. In toluene/anisole 30 : 70 and in neat anisole, a further slight increase in dielectric constant makes ICT a competitive pathway to the biexcitonic ^{1}A population, showing an extreme sensitivity of the system to the medium polarity.

Temperature effects on the emission spectra in toluene were retrieved from the previous study.[21] By plotting the ratio of the fluorescence intensity of the singlet 1^1B and 2^1A states (namely I_F at 22 200 and 18 180 cm^{-1}, respectively), $\ln[I_F(1^1\text{B})/I_F(2^1\text{A})]$, as

a function of reciprocal temperature ($1/T$) in the 353–280 K range, an energy barrier for the 1^1B to 2^1A crossing of 625 cm^{-1} was obtained in toluene using the slope of the Arrhenius-like linear treatment (Fig. S20‡).

Concentration effects

No aggregation was found to occur in the ground-state **1** under the experimental conditions: no concentration effect is observed on the absorption spectra recorded in toluene at different concentrations (Fig. S15‡). Similarly, no concentration effect is observed on the emission spectral shape, apart from some decrease of the fluorescence intensity at the blue side due to the inner filter effect (Fig. S15‡), upon increasing the concentration by almost two orders of magnitude (between *ca.* 10^{-6} and 10^{-4} M) focusing on the absence of fluorescent excimers.

However, the triplet quantum yield (Φ_T) measured by ns-TA increased with the solution concentration and reached values close to 200% ($\Phi_T = 1.9 \pm 0.1$) in 2×10^{-4} M solutions.

The fs-TA experiments were also performed at different concentrations for **1** in toluene (Table S11‡) under the same experimental conditions. No concentration effect was revealed for the short-lived relaxed 1^1B transient. Faster dynamics was observed for the longer-lived 2^1A transient in concentrated solutions. Furthermore, the fs-TA data obtained by employing sapphire and CaF_2 crystals for concentrated solutions in toluene (8×10^{-5} M) were normalized and merged. The goal was to have spectral data showing both the Excited State Absorption (ESA) peaks and the Ground State Bleach (GSB) signal. However, the complete data matrix analysis according to a procedure already described in the literature (Fig. S16–S19 and Table S12‡)[35,36] did not provide a reliable triplet yield value since in the present case, only the GSB tail could be observed. In fact, we were unable to generate white light in correspondence with the GSB peak, causing large errors. Nevertheless, this procedure suggests a high triplet state production in agreement with the quantum yield determined by ns laser flash-photolysis measurements.

Triangular cuts through potential energy surfaces

Geometry optimizations employing XMCQDPT2 in ANO-S-VDZP basis set[37] (DZ) led to potential energy minima of 1^1A, 2^1A, and 1^1B states. These geometries preserve the original point group symmetry within the margin of numerical error. 1^1A, 2^1A, and 1^1B minima are the vertices (black, red, and blue triangles, resp., in Fig. 5 and 6) that generate a triangular cut through the excited- and ground-state potential energy surfaces (PES).

XMCQDPT2 in ANO-L-VTZP basis set (TZ)[38] single-point results at these vertices for both **1a** and **1s** were almost identical (Table 2 and S1‡). The results accurately predict both observed stationary absorption and transient emission spectra. Table S2‡ provides description of the states of interest as major configurations in zeroth-order XMCQDPT2/TZ states.

Fig. 5 shows the first two edges of the triangular cut of the PES. The XMCQDPT2/TZ calculations produce only negligible difference between **1a** and **1s** PES (full and dashed lines,

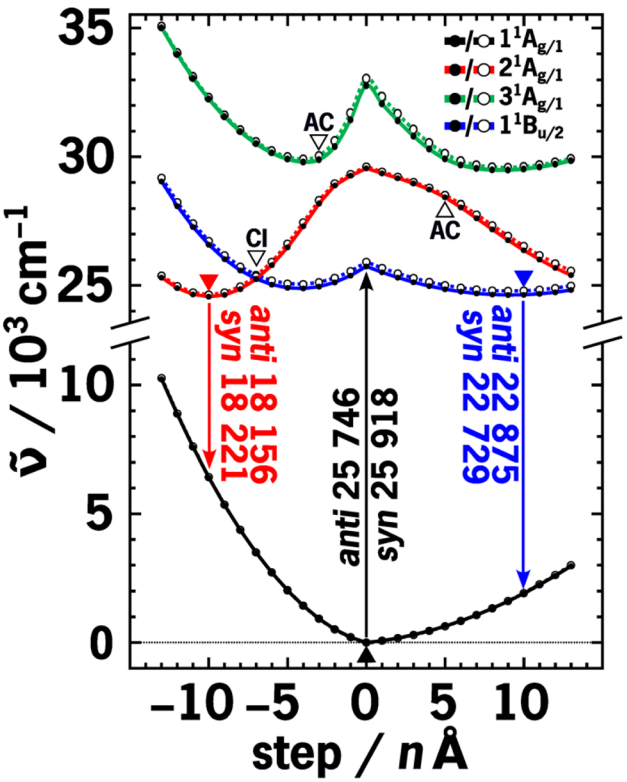

Fig. 5 Cuts through XMCQDPT2/ANO-L-VTZP ground-state and three lowest singlet-excited-state potential energy surfaces of **1a** (full line with full circles) and **1s** (dotted line with empty circles). The energy paths lead from the XMCQDPT2/ANO-S-VDZP optimal geometries (color-coded triangles) of the ground state (1^1A) to optimal geometries of the 1^1B (step > 0), and 2^1A (step < 0). Empty triangles denote approximate positions of conical intersection (CI) and avoided crossings (AC). Energy differences are shown by color-coded arrows. Each step represents a single-point calculation. Step sizes differ for each linear transect toward an optimal geometry to allow for an overlapping figure and comparison; $n(2^1A_g) = 0.216$, $n(2^1A_1) = 0.305$, $n(1^1B_u) = 0.159$, and $n(1^1B_2) = 0.205$.

respectively). The ground state energies of both conformers throughout the linear transect are almost perfectly degenerate.

At the optimal ground state geometries of both **1a** and **1s**, the energy of the 2^1A is well-above that of 1^1B by ~4000 cm^{-1}. At 2^1A optimal geometry, the ^{1}A state lies below the ^{1}B state by ~2000 cm^{-1}. At the 1^1B optimal geometry, the ^{1}B state lies below the ^{1}A state by ~1700 cm^{-1}. Finally, 2^1A and 1^1B minima of energy are effectively degenerate at this level of theory (ΔE < 0.02 eV).

Fig. 6 finishes the last edge of the outlined triangle connecting the 2^1A and 1^1B vertices. It shows the energy barrier between the two states of both **1a** and **1s** at XMCQDPT2/TZ to be practically identical in both directions at about 530 cm^{-1} (~1.5 kcal mol^{-1}).

Modelling transient absorption spectra

Further XMCQDPT2/DZ geometry optimizations of the lowest triplet state led to both minima that preserve their original point group for **1a** and **1s** (Table S4‡) and one with a lower

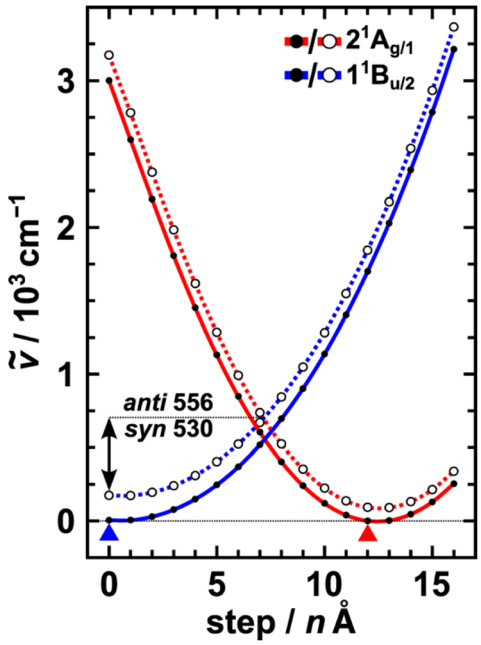

Fig. 6 Cuts through XMCQDPT2/ANO-L-VTZP singlet-excited-state potential energy surfaces of **1a** (full line with full circles) and **1s** (dotted line with empty circles). The lowest energy paths lead between the XMCQDPT2/ANO-S-VDZP 1^1B and 2^1A optimal geometries (color-coded triangles). Energy differences between 1B states and the conical intersections are shown as a double-headed arrow. Each step represents a single-point calculation. Step sizes differ for each linear transect to allow for an overlapping figure and comparison; $n(2^1A_g) = 0.071$ and $n(2^1A_1) = 0.105$.

Table 2 Observed and XMCQDPT2/ANO-L-VTZP calculated vertical (de)excitation energies and oscillator strengths of the two lowest singlet excited states of **1a**

Geom.[a]	ΔE/eV	ΔE/cm^{-1}	ΔE_{obs}[b]/cm^{-1}	f[c,d]
Transition: $1^1A_g \rightarrow 2^1A_g$				
1^1A_g	3.66	29 554	—	0.00, *0.00*, **0.00**
2^1A_g	2.25	18 156	18 200	0.00, *0.00*, **0.00**
1^1B_u	3.03	24 462	—	0.00, *0.00*, **0.00**
Transition: $1^1A_g \rightarrow 1^1B_u$				
1^1A_g	3.19	25 746	25 200	1.80, *1.85*, **2.37**
2^1A_g	2.50	20 184	—	1.99, *1.95*, **2.85**
1^1B_u	2.82	22 729	21 100	1.95, *1.97*, **2.63**

[a] State at whose equilibrium geometry calculations were performed. [b] See Fig. 2. [c] CASSCF results in roman, XMCQDPT2 results in italics, XMS-CASPT2 results in bold. [d] Evaluated using eqn (S3).

symmetry (C_s) for **1a** (Tables S5 and S6‡). The states of experimental interest and their transitions were identified within the point groups with their irreducible representations as $1^3B \rightarrow 2^3A$ for triplet and $2^1A \rightarrow 3^1B$ and $1^1B \rightarrow 5^1A$ for singlet transitions. These were also the only strongly allowed transitions within the range of state-averaging. Table S4‡ provides description of the states of interest as major configurations in zeroth-order XMCQDPT2/TZ states (Table 3).

Table 3 Observed and XMCQDPT2/ANO-L-VTZP calculated vertical excitation energies and oscillator strengths of the triplet and singlet transients of interest at their respective optimal geometries of **1a**[a]

Transition	ΔE/eV	ΔE/cm^{-1}	ΔE_{obs}[b]/cm^{-1}	f[c,d]
$1^3B_u \rightarrow 2^3A_g$	2.07	16 693	15 700	1.61, *1.73*, **1.77**
$2^1A_g \rightarrow 3^1B_u$	2.07	16 730	15 700	1.67, *1.76*, **2.19**
$1^1B_u \rightarrow 5^1A_g$	1.58	12 762	13 500	2.98, *3.01*, **3.52**

[a] See Table S2 for the **1s** results. [b] See Fig. 3 and 4. [c] CASSCF results in roman, XMCQDPT2 results in italics, XMS-CASPT2 results in bold. [d] Evaluated using eqn (S3).

The theoretical results (Table 3) come with a similar blue shift of roughly 1000 cm^{-1} for the energy gaps of the triplet and biexciton species and with a red shift of roughly 800 cm^{-1} for the single-excited state. The calculated lowest 2^1A and 1^3B absorption bands have identical energy gap (energy difference <0.01 eV). On the other hand, the ratio of the calculated oscillator strengths between 2^1A and 1^3B differs qualitatively depending on the employed method: CASSCF/TZ and XMCQDPT2/TZ return ratios close to 1 : 1, while XMS-CASPT2/DZ a ratio of 1.24 : 1 in favor of the singlet $2^1A \rightarrow 1^1B$ transition.

Adiabatic excitation energies of singlet, triplet, and quintet species

Finally, XMCQDPT2/DZ geometry optimizations of the 1^5A_g states of **1a** and **1s** yielded C_{2h}- and C_{2v}-symmetric geometries, respectively. Ground-state adiabatic excitation energies of C_{2h}- and C_{2v}-symmetric excited-state geometries of all studied multiplicities were calculated at XMCQDPT2/TZ.

The energies in eV are for singlet species: 3.05 eV for both 2^1A_g and 1^1B_u; 3.06 for 2^1A_1; and 3.07 1^1B_2; and for higher calculated multiplicities: 1.78 for both the 1^3B_u and 1^3B_2; 3.95 and 3.94 for 3^3B_u and 3^3B_2, respectively; and 4.59 eV for both 1^5A_g and 1^5A_1.

Localized frontier molecular orbital analysis (LFMO)

Following the LFMO analysis (Fig. 7, eqn (S1), (S2), and Fig. S7‡),[11,39] the $^1(T_1T_1)$ configuration is not present in the 2^1A_g state at ground state geometry (Table S3‡). It is instead defined almost solely by in-phase combination of single-excited species $S_1S_0 + S_0S_1$ configurations. The 3^1A_g state contains the sought leading $^1(T_1T_1)$ configuration with a small admixture of an out-of-phase intramolecular charge-transfer state (ICT) $^1(D^+D^- - D^-D^+)$. It lies in close proximity and steadily mixes with 2^1A_g. Their interaction increases towards an avoided crossing (Fig. 5) – that takes place before the conical intersection with 1^1B_u. Only after this avoided crossing, the $^1(T_1T_1)$ becomes the leading configuration of 2^1A_g and the in-phase $S_1S_0 + S_0S_1$ becomes the leading configuration of 3^1A_g. 1^1B_u keeps its leading out-of-phase localized single-excitation S_1S_0–S_0S_1 character with an intermix of an in-phase ICT $^1(D^+D^- + D^-D^+)$ throughout all the linear transects.

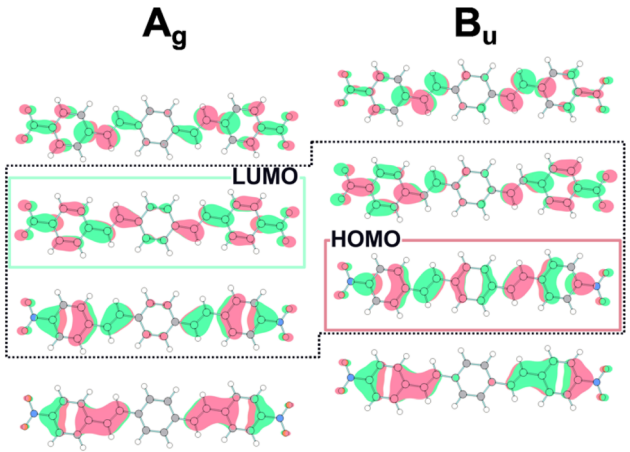

Fig. 7 Orbitals of **1a** in 1^1A_g state geometry resulting from a single-point CASSCF calculation in ANO-L-VTZP basis set split according to their symmetries and ordered qualitatively by their energies – most stable at the bottom. Red and green boxes denote HOMO and LUMO, respectively; dotted box denotes the minimal physically relevant active space employed for localized frontier molecular orbital analysis (see eqn (S1), (S2) and Fig. S7‡). Orbitals of geometries at different states, of **1s**, and in ANO-S-VDZP basis set used for geometry optimizations are qualitatively similar in the used π-orbital space.

As for the transient species, the 1^3B_u state is defined by a leading in-phase $S_0T_1 + T_1S_0$ configuration with an out-of-phase ICT $^3(D^+D^- - D^-D^+)$ admixture. The final state 2^3A_g is defined by a leading in-phase ICT $^3(D^+D^- + D^-D^+)$. In turn, the singlet 3^1B_u is defined by a leading out-of-phase ICT $^1(D^+D^- - D^-D^+)$ for the singlet transition from 2^1A_g. 5^1A_g is a mixture of the A symmetry configurations of interest – S_0S_0, $^1(D^+D^- + D^-D^+)$, $S_1S_0 + S_0S_1$, and $^1(T_1T_1)$.

Finally for the higher spin multiplicity states of particular interest to SF, the 3^3B_u is the overall triplet projection of the triplet biexciton $^3(T_1T_1)$ and 1^5A_g represents the quintet $^5(T_1T_1)$.

The **1s** characters of states of interest behave equivalently as their canonical wavefunctions share the configurations and weights with **1a** (Tables S3 and S4‡).

Discussion

In the whole series of phenylenevinylene oligomers, we would expect the analogs of the 1^1B_u and 2^1A_g excited states of all-*s-trans* conformers of all-*trans* polyenes to be the lowest allowed and lowest forbidden excited state, respectively. The former corresponds to the initial singlet exciton and the latter to the biexciton. Indeed, in the literature, low-lying singlet excited states of A_g nature that are not allowed in absorption have been found to show multiexciton character and to mediate intramolecular SF.[1,3,39–45]

In the following discussion, we interweave our theoretical and experimental efforts and wish to: (i) elucidate the nature of these states; (ii) describe the observable transitions leading to the dual fluorescence; (iii) decide whether the formation of 2^1A states in **1** is the first half of SF or a simple internal conversion (IC); and (iv) probe, whether there are other ways of increasing the triplet quantum yields.

Properties of the conformers

The properties of the s-*anti* (**1a**) and s-*syn* (**1s**) conformers are very similar, but their symmetry properties differ (Fig. 1).[46] The optimized geometries are planar and effectively energetically degenerate, as anticipated from their equal abundance in solution and further corroborated by the absence of excitation wavelength effects on the photobehavior. The allowed $\pi\pi^*$ absorption and emission will be mostly in-plane polarized. The **1a** conformer is centrosymmetric (C_{2h}) and one-photon transitions from the *gerade* (g) symmetry ground state to its *g* excited states will be forbidden, whereas those to its *ungerade* (u) states will be allowed. They are to be polarized along both the long and short molecular axes.

The non-centrosymmetric **1s** conformer (C_{2v}) has an additional plane of symmetry. One-photon transitions from its totally symmetric (A_1) ground state to its A_1 excited states will be polarized along the short molecular axis and will be relatively weakly allowed. On the other hand, those to its totally antisymmetric (B_2) excited states will be polarized along the long molecular axis. Following the length of the molecule, these should be strongly allowed. Finally, the out-of-plane allowed transitions to B_1 are not considered, as those states are not represented within the π-orbital space considered by our study.[47] All these symmetry-based qualitative observations are consistent with our quantitative multireference calculations.

Nature of the excited states and dual emission

The intense absorption peak observed at ~25 200 cm^{-1} is assigned to the canonical HOMO → LUMO transition at 25 746 and 25 918 cm^{-1} in **1a** ($1^1A_g \rightarrow 1^1B_u$) and **1s** ($1^1A_1 \rightarrow 1^1B_2$), respectively, and its polarization is close to or exactly along the long molecular axis. A second, higher-energy transition is predicted to produce a state described by a mixture of HOMO+1 → LUMO and HOMO → LUMO−1 configurations of 2^1A_g symmetry in **1a** and 2^1A_1 symmetry in **1s**. The transition is thus forbidden in the former and very weakly allowed in the latter. In summary, the absorption spectrum is dominated by a strong absorption band due to 1A → 1B.

LFMO analysis reveals that the 2^1A states at the equilibrium ground-state geometries are in-phase coupled localized excitation ($S_1S_0 + S_0S_1$) counterparts of the out-of-phase 1^1B (S_1S_0–S_0S_1). Their considerable energy gap suggests strong coupling between these localized excitons. This coupling weakens towards 1^1B optimal geometry and conversely strengthens towards 2^1A optimum. This is in line with the view of the 1^1B structure as the one closer to the diradicaloid one (Fig. 8).

The above explanation forgoes the interaction of the 3^1A state that becomes important closer to the select optima of both the excited states of interest (Fig. 5). In both directions, the interaction produces an avoided crossing where there is a drastic change in the nature of the 2^1A state. Just after this crossing, the 2^1A becomes the sought $^1(T_1T_1)$ with an admixture of an out-of-phase ICT $^1(D^+D^- - D^-D^+)$.

At the respective minima of energies of both the lowest A and B excited states, our calculations predict the 2^1A states to be slightly lower in energy than the 1^1B states (Fig. 6). Since it thus

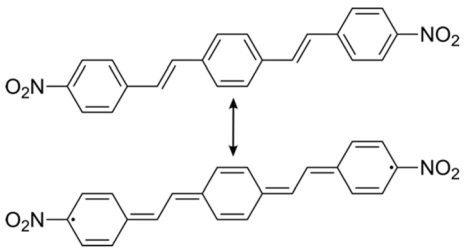

Fig. 8 Resonance structures of **1**: canonical (top) and diradical (bottom).

represents the lowest energy spin-allowed diabatic transition, the corresponding forbidden 2^1A_g or almost forbidden 2^1A_1 excited state is labeled S_1 for the purpose of the following analysis and the allowed 1^1B_u or 1^1B_2 excited state in one or the other conformer then is S_2. However, we note the energy differences to be within the method's margin of error.

If the standard Kasha rule is followed strictly, the fluorescence spectrum would be expected to occur from the relaxed S_1 state (2^1A), enabled by the borrowing of vibronic intensity and polarization from the allowed 1^1B states.[48] Conceivably, however, thermal equilibration of populations of the S_1 and S_2 states would allow some of the fluorescence to originate from the S_2 (1^1B) state. The dual emission experimentally evidenced by FUC and a consideration of the observed fluorescence lifetimes and derived quantum yields suggests that the radiative lifetime of the measured fluorescence is on the order of 2 and 250 ns for S_2 and S_1, respectively. This suggests that the bulk of the emission occurs from the allowed 1^1B states, thermally equilibrated with 2^1A states, thus breaking the Kasha rule.

The predicted emission wavelengths for both 1^1B and 2^1A are in an excellent agreement with the experimentally observed ones, further supporting the notion. We only observe a small systematic red shift between the experimental and calculated values for A → A transitions and a blue shift for A → B for both emission and absorption spectra. The latter can be mostly attributed to a missing inclusion of the solvent and generally to the systematic error of XMCQDPT2, which is well-within the expected margins of a PT2-based theory in TZ basis.[38]

The thermal equilibration hypothesis is further substantiated by the calculated barrier of $1^1B \rightarrow 2^1A$ transition in an excellent agreement with the presence of an activated pathway for the dual emission – as experimentally derived by the temperature effect on fluorescence properties. Owing to the $^1(T_1T_1)$ configuration of 2^1A as described by the calculations, we claim to have observed the proper emission of the double triplet[49–53] in addition to the more conventional emission from the allowed 1^1B state.

Furthermore, we focus on the deviation between the absorption and excitation spectra (Fig. 2), not dissimilar to the measured spectra of *trans*-styrylpyridines, azastilbenes, and *trans*-1,2-diarylethylenes.[54–57] Herein, the explanation given above and the notion of breaking the Kasha rule could handily explain the discrepancy. At low energies, the excited **1** ends up locked in the highly emissive S_2 (1^1B) state, while it easily overcomes the barrier at higher excitation energies and ends up in the less emissive S_1 (2^1A). Therefore, the weight of the poorly fluorescent double triplet state is a little higher when exiting at the blue side of the absorption spectrum.

Kinetic modelling of the first half of SF

The fs-TA measurements allowed us to observe the initially produced short lived 1^1B states (17 ps), responsible for the TA at ~13 600 cm^{-1} and the higher energy emission at ~21 100 cm^{-1}. We then observed a decay to 2^1A, responsible for the TA at 15 600 cm^{-1} and the lower energy emission at ~18 000 cm^{-1}. From a detailed kinetic study of stilbenes[27] and our previous study of 1,4-diarylbenzene derivatives,[58] we expect no internal conversion to S_0 to compete in the 1^1B deactivation. In fact, at low temperatures, only two main decay pathways were shown to be operative: fluorescence ($k_F = 5.5 \times 10^8$ s^{-1}; the same as calculated at room temperature) and ordinary intersystem crossing (ISC) with a k_{ISC} of 5.8×10^8 s^{-1},[21] which is comparable to that reported in other 1,4-diarylbenzene derivatives.[58] Similarly, it is assumed that 1^1B is too short lived to undergo ISC significantly at room temperature – the triplet formation is therefore due to a different deactivation pathway. Moreover, the photoisomerization in the singlet manifold was reported to be negligible for **1** ($\Phi_{ISO} = 0.0022$) in toluene at room temperature.

In fact, it was not possible to directly experimentally distinguish the rise of the 2^1A from the rise of the relaxed triplet 1^3B due to the overlapping TA spectra. We could only directly observe a rise time of 16.9 ps at 15 600 cm^{-1} simultaneous to the 1^1B decay. However, at least a very low quantum yield, comparable to that found for the fluorescence (0.01), can be expected for the $1^1B \rightarrow 1^3B$ ordinary ISC. Consequently, 1^1B mainly decays to the coupled biexciton 2^1A (k_{SF}) with an almost unitary yield.

Finally, slow radiative conversion of 2^1A to S_0 (k_F) and its non-radiative conversion to 1^3B (k_T), possibly followed by photoisomerization in the triplet manifold[21] and to the ground state S_0 (k_G), deplete the population of 2^1A and terminate all fast photophysical processes. The kinetic scheme for the excited state decay of **1** in toluene at room temperature shown in Fig. 9 summarizes the proposed model.

Toward higher triplet yields

The presence of an ICT state in **1**, a push–pull quadrupolar compound, was evidenced as an intermediate transient species between 1^1B_u and 2^1A_g in toluene/anisole mixtures. In net anisole and in more polar solvents as well, it became the lowest singlet state in fs-TA measurements (see Fig. S14, Table S10‡ and ref. 21). Therefore in the less polar toluene, the ICT state could act as a high-energy virtual state favoring SF through an ICT-mediated superexchange mechanism,[1,22,24,59–61] as observed in fluorene derivatives in solution,[24,62] and in solution, thin films and crystals of other molecules.[23,53,63–65] This is coherent with the LFMO analysis highlighting the admixture of ICT states in the 2^1A wavefunction *in vacuo*. It is conceivable that these would become the major contribution when subject to an electrostatic field of polar solvent molecules, forming a separate, real state, as observed by fs-TA in polar solvents (Table

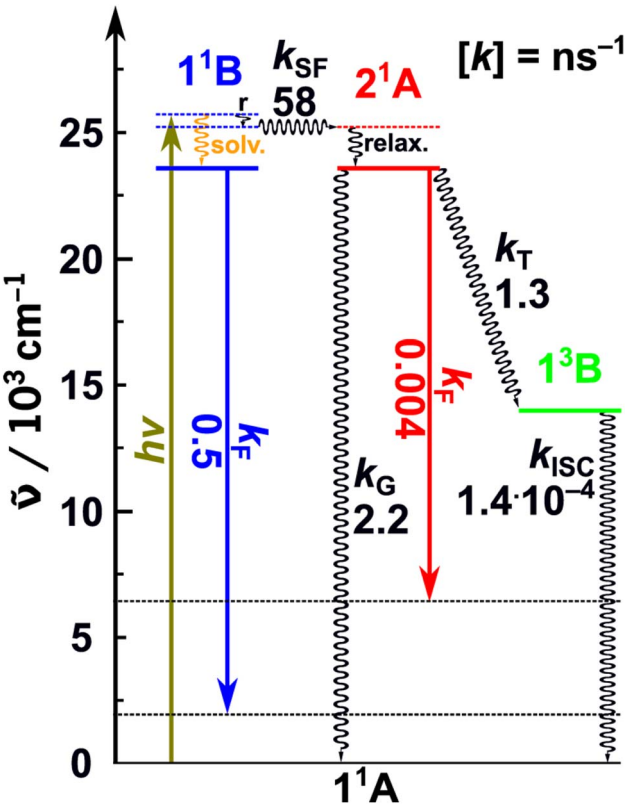

Fig. 9 Color-coded Jabłonski diagram with a kinetic scheme for excited state decay of **1** in toluene at room temperature. Thick, full lines denote equilibrium (adiabatic) energies relative to the equilibrium energy of the ground state. Thin, dashed lines denote higher energy states of the same electronic state. Straight and wavy arrows denote radiative and non-radiative processes, respectively. Rate constants (k) with respective values below in ns^{-1}. Energies obtained compositely from both theory and experiment.

S10‡). This real charge-separated state then becomes a trap state and a competitive pathway to SF – much like we observe in more polar solvents here or that we previously observed in crystals of indigo derivatives.[66,67]

However, the high sensitivity of the photobehavior of **1** to small changes in solvent polarizability suggests the calculated high interaction energy between the two triplets[68–70] within the $^1(T_1T_1)$ *in vacuo* to be much smaller in polarizable solvents. In fact, the surprising resemblance of the absorption spectra of 2^1A and 1^3B – with only 0.009 eV ($\sim$70 cm^{-1}) between their observed TA maxima – could be the sign of a small interaction between the two triplets inside the $^1(T_1T_1)$ state. In a previous paper about SF in conjugated stilbenoid compounds,[71] this similarity between the spectra of 1^3B and 2^1A and, in particular, the energy difference between their maxima, has been related to the interaction strength between the two triplets within the double triplet complex. Indeed, the spectral difference obtained by comparison of the TA peaks of the biexcitonic 2^1A and independent triplet states was found to be in a remarkable trend with the observed Φ_T and triplet separation rate constant.

Furthermore, the resemblance of triplet and triplet biexciton spectra was previously discussed by Barford[72] and it is congruent with our LFMO analysis of **1**. Both transitions ($2^1A \rightarrow 3^1B$ and $1^3B \rightarrow 2^3A$) are transitions from our diabatic state of interest, T_1 or $^1(T_1T_1)$, with the admixture of ICT to a state almost purely consisting of the opposite-phase ICT. It was shown that the contribution to the intensity of this transition in dipole approximation lies solely on the transition dipole between the ICT and the opposite-phase ICT. Therefore, the transition dipoles from the triplet and triplet biexciton configurations to the ICT configuration are negligible or completely vanishing.

Ultimately, we observe an extraordinary jump in Φ_T in high-concentration toluene solutions of **1** nearing or even reaching 200%. These results were confirmed by two independent determinations, with the Φ_T values being accurately measured by ns-TA and confirmed by an estimate resulting from analysis of the fs-TA data (see Section 7 of the ESI and Fig. S16–S20‡) based on the method outlined by Carmichael and Hug[35] and successfully adapted for SF materials.[36,64,73] These results point to an efficient triplet separation in solution despite the large endothermicity ($\Delta E^{adibatic}(2^1A) < 2\Delta E^{adibatic}(1^3B)$, see Fig. 9) and considerable splitting between T_1T_1 states of different multiplicities calculated *in vacuo* in a single molecule. We surmise that the possible mechanism must be based on intermolecular spatial triplet separation, which was shown to drive even largely endothermic SF in chromophore oligomers.[74] However, the concentration effects on the absorption spectrum do not show the presence of aggregates, which defies the classically asserted need for long-range order. It is still conceivable to suggest a spatial triplet separation based on triplet energy transfer: $^1(T_1T_1) + S_0 \rightleftarrows T_1 + T_1$, as described and observed in neatly ordered solid aggregates.[3,75–83] Such dissociation has been reported only in the case of dimer systems of pentacene and tetracene chromophores in highly concentrated solutions (10^{-3} M)[84] by collisional exciton transfer and speculated in the case of fluorene nitro derivatives in mildly concentrated solution ($\leq 10^{-4}$ M), through a very efficient superdiffusional mechanism.[62] In this mechanism, electronic coupling and entropic contributions should play a key role in speeding up the energy transfer process.[83,85–87] The largely endoergic path obtained from the theory may be further diminished by high entropy. In ref. 62, an intermediate force coupling regime has been hypothesized to be responsible for the ultrafast bimolecular energy transfer.[88–92] Within this framework, one might speculate a peculiar "super diffusional" energy transfer occurring from the donor (a weakly bound triplet within the $^1(TT)$ state) to the acceptor (a second ground state molecule of the same nature, thus with large resonance energy) to produce an additional T_1 through a super exchange mechanism. Similar to what was observed for the electron transfer process, the solvent might also act as the mediator for this unconventional energy transfer process,[93–96] thus participating in the $^1(TT)$ separation. The employed theory treats electronic energy alone and thus the true difference of Gibbs energy of triplet separation is unknown.

However, a small contribution of intermolecular SF mechanism to the triplet production cannot be completely ruled out at the highest concentrations due to the poor solubility of the compound.

Finally, it is curious to see that the common denominator for both the in-solution SF-active push–pull compounds, **1** and the

previously examined fluorene derivative[62] is the nitro group. Considering the established synthetic route, we speculate that it might be worthwhile to explore alternative electron-withdrawing groups. The effort could yield in-solution SF-viable compounds with distinct physicochemical properties tailored for specific use cases.[97–99]

Conclusion

We have intertwined both steady-state and ultrafast absorption and emission measurements in ns and fs regimes with high-level *ab initio* XMQCDPT2 to probe and explain the unusual dual-emission and SF mechanism for the triplet production of **1** in toluene solutions.

The model compound **1** here investigated has shown dual fluorescence, from the allowed 1^1B state of HOMO → LUMO nature and the forbidden 2^1A state of $^1(T_1T_1)$ biexciton nature. The biexciton state exhibits a behavior intermediate between the strongly coupled triplet pair and uncoupled triplet pair. Indeed, the experimentally observed $^1(T_1T_1) \rightarrow {}^1(T_1T_x)$ ($2^1A \rightarrow 3^1B$) absorption by fs-TA measurements is very similar to the $T_1 \rightarrow T_x$ ($1^3B \rightarrow 2^3A$) absorption of a lone triplet state, but its intensity is only higher by a factor of 1.5, whereas a factor of 2 would be expected for two truly isolated triplets.

The combined experimental and theoretical approach unveiled and described an activated pathway of intramolecular $^1(T_1T_1)$ biexciton generation. Solvent polarity studies point to a possible through-charge-transfer-state (superexchange) mechanism. Employing ns time resolved measurements, we obtained triplet yield in concentrated toluene solutions approaching 200%. Since in intramolecular SF the two triplet excitations should be located on the same molecule, the completion of the SF process is typically harder to achieve, especially in small molecules; we thus suspect a previously hypothesized superdiffusional intermolecular mechanism to aid in triplet separation, namely, the presence of nearby molecules in concentrated solutions may allow sharing of a triplet without losing the other one by an energy transfer process [$^1(T_1T_1) + S_0 \rightarrow T_1 + T_1$]. The entropy factors and spatial separation are likely the driving force for the second half of the SF process in solution.

Given the exceptional SF behavior here uncovered in this small dinitro-distyrylbenzene molecule, further studies are in progress to explore the effect of alternative electron-withdrawing groups on the SF energetics and dynamics to provide application-specific properties.

Data availability

The data supporting this article have been included as part of the ESI.‡

Author contributions

The manuscript was written through contributions of all authors. Letizia Mencaroni: formal analysis, data curation, investigation, methodology, visualization, writing – original draft; Alexandr Zaykov: conceptualization, data curation, formal analysis, investigation, software, visualization, writing – original draft, review & editing; Benedeta Carlotti: conceptualization, data curation, formal analysis, funding acquisition, investigation, writing – original draft, review & editing; Fausto Elisei: data curation, software, writing – original draft; Guillaume Bastien: methodology, validation, writing – original draft; Raimondo Germani: methodology, investigation, writing – original draft; Zdeněk Havlas: conceptualization, funding acquisition, project administration, resources, supervision; Anna Spalletti: conceptualization, formal analysis, funding acquisition, investigation, project administration, resources, supervision, writing – original draft, review & editing; Josef Michl: conceptualization, funding acquisition, project administration, resources, supervision, writing – original draft.

Conflicts of interest

The authors declare no competing financial interest or other conflicts.

Acknowledgements

Work in Perugia has been funded by the European Union – NextGenerationEU under the Italian Ministry of University and Research (MUR) National Innovation Ecosystem grant ECS00000041 – VITALITY. We acknowledge Università degli Studi di Perugia and MUR for support within the project Vitality. L. M. acknowledges the Valhalla project – "Perovskite solar cells with enhanced stability and applicability" and Istituto di Scienze e Tecnologie Chimiche (SCITEC) "Giulio Natta". B. C. acknowledges MUR financial support under the PRIN 2022 program, grant no. 2022RRFJC4. Work in Prague was supported by the Institute of Organic Chemistry and Biochemistry (RVO: 61388963) and GAČR grant 19-22806S. Work in Boulder was supported by the U.S. Department of Energy, Office of Basic Energy Sciences, Division of Chemical Sciences, Biosciences, and Geosciences, under award number DE-SC0007004. A. Z. wishes to express his gratitude toward Dr Jae Woo Park for the provided BAGEL code and support and toward Dr Jiří Kaleta for the fruitful discussions and provided help.

References

1 M. B. Smith and J. Michl, *Chem. Rev.*, 2010, **110**, 6891–6936.
2 M. B. Smith and J. Michl, *Annu. Rev. Phys. Chem.*, 2013, **64**, 361–386.
3 K. Miyata, F. S. Conrad-Burton, F. L. Geyer and X. Y. Zhu, *Chem. Rev.*, 2019, **119**, 4261–4292.
4 W. Shockley and H. J. Queisser, *J. Appl. Phys.*, 1961, **32**, 510–519.
5 M. C. Hanna and A. J. Nozik, *J. Appl. Phys.*, 2006, **100**, 074510.
6 B. Daiber, K. van den Hoven, M. H. Futscher and B. Ehrler, *ACS Energy Lett.*, 2021, **6**, 2800–2808.
7 A. J. Baldacchino, M. I. Collins, M. P. Nielsen, T. W. Schmidt, D. R. McCamey and M. J. Y. Tayebjee, *Chem. Phys. Rev.*, 2022, **3**, 021304.

8 T. Sharma, M. A. Afroz and S. Satapathi, *ACS Photonics*, 2024, **11**, 3922–3932.
9 K. E. Smyser and J. D. Eaves, *Sci. Rep.*, 2020, **10**, 18480.
10 A. Yamauchi, K. Tanaka, M. Fuki, S. Fujiwara, N. Kimizuka, T. Ryu, M. Saigo, K. Onda, R. Kusumoto, N. Ueno, H. Sato, Y. Kobori, K. Miyata and N. Yanai, *Sci. Adv.*, 2024, **10**, eadi3147.
11 R. P. Hosteny Jr, T. H. Dunning, R. R. Gilman, A. Pipano and I. Shavitt, *J. Chem. Phys.*, 1975, **62**, 4764–4779.
12 B. G. Levine, C. Ko, J. Quenneville and T. J. Martínez, *Mol. Phys.*, 2006, **104**, 1039–1051.
13 J. M. Leng, S. Jeglinski, X. Wei, R. E. Benner, Z. V. Vardeny, F. Guo and S. Mazumdar, *Phys. Rev. Lett.*, 1994, **72**, 156–159.
14 R. Österbacka, M. Wohlgenannt, D. Chinn and Z. V. Vardeny, *Phys. Rev. B:Condens. Matter Mater. Phys.*, 1999, **60**, R11253–R11256.
15 R. Österbacka, M. Wohlgenannt, M. Shkunov, D. Chinn and Z. V. Vardeny, *J. Chem. Phys.*, 2003, **118**, 8905–8916.
16 F.-T. Luo, Y.-T. Tao, S.-L. Ko, C.-H. Chuen and H. Chen, *J. Mater. Chem.*, 2002, **12**, 47–52.
17 K. Baatout, C. Mahmoudi, M. Laajimi, F. Ibn EL Hadj Rhouma, N. Smida and M. Majdoub, *Opt. Mater.*, 2023, **146**, 114588.
18 Y. Shimomura, K. Igawa, S. Sasaki, N. Sakakibara, R. Goseki and G. Konishi, *Chem.–Eur. J.*, 2022, **28**, e202201884.
19 E. Marri, D. Pannacci, G. Galiazzo, U. Mazzucato and A. Spalletti, *J. Phys. Chem. A*, 2003, **107**, 11231–11238.
20 E. Marri, F. Elisei, U. Mazzucato, D. Pannacci and A. Spalletti, *J. Photochem. Photobiol., A*, 2006, **177**, 307–313.
21 B. Carlotti, F. Elisei, U. Mazzucato and A. Spalletti, *Phys. Chem. Chem. Phys.*, 2015, **17**, 14740–14749.
22 E. Busby, J. Xia, Q. Wu, J. Z. Low, R. Song, J. R. Miller, X.-Y. Zhu, L. M. Campos and M. Y. Sfeir, *Nat. Mater.*, 2015, **14**, 426–433.
23 B. S. Basel, J. Zirzlmeier, C. Hetzer, S. R. Reddy, B. T. Phelan, M. D. Krzyaniak, M. K. Volland, P. B. Coto, R. M. Young, T. Clark, M. Thoss, R. R. Tykwinski, M. R. Wasielewski and D. M. Guldi, *Chem*, 2018, **4**, 1092–1111.
24 L. Mencaroni, B. Carlotti, F. Elisei, A. Marrocchi and A. Spalletti, *Chem. Sci.*, 2022, **13**, 2071–2078.
25 A. A. Granovsky, *J. Chem. Phys.*, 2011, **134**, 214113.
26 I. N. Ioffe and A. A. Granovsky, *J. Chem. Theory Comput.*, 2013, **9**, 4973–4990.
27 I. N. Ioffe, M. Quick, M. T. Quick, A. L. Dobryakov, C. Richter, A. A. Granovsky, F. Berndt, R. Mahrwald, N. P. Ernsting and S. A. Kovalenko, *J. Am. Chem. Soc.*, 2017, **139**, 15265–15274.
28 J. W. Park, *J. Chem. Theory Comput.*, 2021, **17**, 6122–6133.
29 W. Park, J. Shen, S. Lee, P. Piecuch, M. Filatov and C. H. Choi, *J. Phys. Chem. Lett.*, 2021, **12**, 9720–9729.
30 J. W. Park, R. Al-Saadon, M. K. MacLeod, T. Shiozaki and B. Vlaisavljevich, *Chem. Rev.*, 2020, **120**, 5878–5909.
31 M. Montalti, A. Credi, L. Prodi and M. T. Gandolfi, *Handbook of Photochemistry*, CRC Press, Boca Raton, 3rd edn, 2006.
32 F. Edhborg, A. Olesund and B. Albinsson, *Photochem. Photobiol. Sci.*, 2022, **21**, 1143–1158.
33 J. J. Snellenburg, S. Laptenok, R. Seger, K. M. Mullen and I. H. M. van Stokkum, *J. Stat. Softw.*, 2012, **49**, 1–22.
34 L. Reynolds, J. A. Gardecki, S. J. V. Frankland, M. L. Horng and M. Maroncelli, *J. Phys. Chem.*, 1996, **100**, 10337–10354.
35 I. Carmichael and G. L. Hug, *J. Phys. Chem. Ref. Data*, 1986, **15**, 1–250.
36 E. A. Margulies, C. E. Miller, Y. Wu, L. Ma, G. C. Schatz, R. M. Young and M. R. Wasielewski, *Nat. Chem.*, 2016, **8**, 1120–1125.
37 J. Almlöf and P. R. Taylor, in *Advances in Quantum Chemistry*, ed. P.-O. Löwdin, J. R. Sabin and M. C. Zerner, Academic Press, 1991, vol. 22, pp. 301–373.
38 F. Plasser, S. A. Mewes, A. Dreuw and L. González, *J. Chem. Theory Comput.*, 2017, **13**, 5343–5353.
39 K. Schulten and M. Karplus, *Chem. Phys. Lett.*, 1972, **14**, 305–309.
40 M. R. Antognazza, L. Lüer, D. Polli, R. L. Christensen, R. R. Schrock, G. Lanzani and G. Cerullo, *Chem. Phys.*, 2010, **373**, 115–121.
41 E. Papagiannakis, J. T. M. Kennis, I. H. M. van Stokkum, R. J. Cogdell and R. van Grondelle, *Proc. Natl. Acad. Sci. U. S. A.*, 2002, **99**, 6017–6022.
42 C. C. Gradinaru, J. T. M. Kennis, E. Papagiannakis, I. H. M. van Stokkum, R. J. Cogdell, G. R. Fleming, R. A. Niederman and R. van Grondelle, *Proc. Natl. Acad. Sci. U. S. A.*, 2001, **98**, 2364–2369.
43 P. Tavan and K. Schulten, *Phys. Rev. B:Condens. Matter Mater. Phys.*, 1987, **36**, 4337–4358.
44 L. Wang, T.-S. Zhang, L. Fu, S. Xie, Y. Wu, G. Cui, W.-H. Fang, J. Yao and H. Fu, *J. Am. Chem. Soc.*, 2021, **143**, 5691–5697.
45 M. Chandross, Y. Shimoi and S. Mazumdar, *Synth. Met.*, 1997, **85**, 1001–1006.
46 A. Gelessus, W. Thiel and W. Weber, *J. Chem. Educ.*, 1995, **72**, 505.
47 R. K. Nesbet, *Proc. R. Soc. London, Ser. A*, 1955, **230**, 322–330.
48 G. Orlandi and W. Siebrand, *J. Chem. Phys.*, 1973, **58**, 4513–4523.
49 C. K. Yong, A. J. Musser, S. L. Bayliss, S. Lukman, H. Tamura, O. Bubnova, R. K. Hallani, A. Meneau, R. Resel, M. Maruyama, S. Hotta, L. M. Herz, D. Beljonne, J. E. Anthony, J. Clark and H. Sirringhaus, *Nat. Commun.*, 2017, **8**, 15953.
50 H. L. Stern, A. Cheminal, S. R. Yost, K. Broch, S. L. Bayliss, K. Chen, M. Tabachnyk, K. Thorley, N. Greenham, J. M. Hodgkiss, J. Anthony, M. Head-Gordon, A. J. Musser, A. Rao and R. H. Friend, *Nat. Chem.*, 2017, **9**, 1205–1212.
51 A. J. Musser and J. Clark, *Annu. Rev. Phys. Chem.*, 2019, **70**, 323–351.
52 S. Lukman, J. M. Richter, L. Yang, P. Hu, J. Wu, N. C. Greenham and A. J. Musser, *J. Am. Chem. Soc.*, 2017, **139**, 18376–18385.
53 D. W. Polak, I. Andrews, E. Salvadori, A. J. Musser, A. Auty, D. Chekulaev, J. A. Weinstein, M. Heeney and J. Clark, *J. Am. Chem. Soc.*, 2025, **147**, 662–668.
54 G. Bartocci and U. Mazzucato, *Chem. Phys. Lett.*, 1977, **47**, 541–544.
55 U. Mazzucato and F. Momicchioli, *Chem. Rev.*, 1991, **91**, 1679–1719.

56 G. Marconi, G. Bartocci, U. Mazzucato, A. Spalletti, F. Abbate, L. Angeloni and E. Castellucci, *Chem. Phys.*, 1995, **196**, 383–393.
57 K. Ogawa, H. Suzuki and M. Futakami, *J. Chem. Soc., Perkin Trans. 2*, 1988, 39–43.
58 S. Ciorba, G. Galiazzo, U. Mazzucato and A. Spalletti, *J. Phys. Chem. A*, 2010, **114**, 10761–10768.
59 Z. Havlas and J. Michl, *Isr. J. Chem.*, 2016, **56**, 96–106.
60 C. E. Miller, M. R. Wasielewski and G. C. Schatz, *J. Phys. Chem. C*, 2017, **121**, 10345–10350.
61 J. C. Johnson, *Commun. Chem.*, 2021, **4**, 1–3.
62 L. Mencaroni, F. Elisei, A. Marrocchi, A. Spalletti and B. Carlotti, *J. Phys. Chem. B*, 2024, **128**, 3442–3453.
63 C. M. Mauck, P. E. Hartnett, E. A. Margulies, L. Ma, C. E. Miller, G. C. Schatz, T. J. Marks and M. R. Wasielewski, *J. Am. Chem. Soc.*, 2016, **138**, 11749–11761.
64 D. Rais, P. Toman, J. Pfleger, U. Acharya, Y. R. Panthi, M. Menšík, A. Zhigunov, M. A. Thottappali, M. Vala, A. Marková, S. Stříteský, M. Weiter, M. Cigánek, J. Krajčovič, K. Pauk, A. Imramovský, A. Zaykov and J. Michl, *ChemPlusChem*, 2020, **85**, 2689–2703.
65 M. Alebardi, C. Munzone, E. Sorbelli, A. Grasso, L. Mencaroni, F. Elisei, C. G. Fortuna, A. Spalletti, C. Bonaccorso and B. Carlotti, *Adv. Funct. Mater.*, 2024, **34**, 2403706.
66 J. L. Ryerson, A. Zaykov, L. E. A. Suarez, R. W. A. Havenith, B. R. Stepp, P. I. Dron, J. Kaleta, A. Akdag, S. J. Teat, T. F. Magnera, J. R. Miller, Z. Havlas, R. Broer, S. Faraji, J. Michl and J. C. Johnson, *J. Chem. Phys.*, 2019, **151**, 184903.
67 J. Kaleta, M. Dudič, L. Ludvíková, A. Liška, A. Zaykov, I. Rončević, M. Mašát, L. Bednárová, P. I. Dron, S. J. Teat and J. Michl, *J. Org. Chem.*, 2023, **88**, 6573–6587.
68 S. N. Sanders, A. B. Pun, K. R. Parenti, E. Kumarasamy, L. M. Yablon, M. Y. Sfeir and L. M. Campos, *Chem*, 2019, **5**, 1988–2005.
69 M. Marcus and W. Barford, *Phys. Rev. B:Condens. Matter Mater. Phys.*, 2020, **102**, 035134.
70 O. Millington, S. Montanaro, A. Sharma, S. A. Dowland, J. Winkel, J. Grüne, A. Leventis, T. Bennett, J. Shaikh, N. Greenham, A. Rao and H. Bronstein, *J. Am. Chem. Soc.*, 2024, **146**, 29664–29674.
71 L. Mencaroni, M. Alebardi, F. Elisei, I. Škorić, A. Spalletti and B. Carlotti, *Phys. Chem. Chem. Phys.*, 2023, **25**, 21089–21099.
72 W. Barford, *Phys. Rev. B:Condens. Matter Mater. Phys.*, 2022, **106**, 035201.
73 P. E. Hartnett, E. A. Margulies, C. M. Mauck, S. A. Miller, Y. Wu, Y.-L. Wu, T. J. Marks and M. R. Wasielewski, *J. Phys. Chem. B*, 2016, **120**, 1357–1366.
74 N. V. Korovina, C. H. Chang and J. C. Johnson, *Nat. Chem.*, 2020, **12**, 391–398.
75 R. D. Pensack, E. E. Ostroumov, A. J. Tilley, S. Mazza, C. Grieco, K. J. Thorley, J. B. Asbury, D. S. Seferos, J. E. Anthony and G. D. Scholes, *J. Phys. Chem. Lett.*, 2016, **7**, 2370–2375.
76 Z. Wang, C. Zhang, R. Wang, G. Wang, X. Wang and M. Xiao, *J. Chem. Phys.*, 2019, **151**, 134309.
77 Z. Wang, H. Liu, X. Xie, C. Zhang, R. Wang, L. Chen, Y. Xu, H. Ma, W. Fang, Y. Yao, H. Sang, X. Wang, X. Li and M. Xiao, *Nat. Chem.*, 2021, **13**, 559–567.
78 V. Abraham and N. J. Mayhall, *J. Phys. Chem. Lett.*, 2021, **12**, 10505–10514.
79 T. S. Volek, M. A. Verkamp, G. N. Ruiz, A. J. Staat, B. C. Li, M. J. Rose, J. D. Eaves and S. T. Roberts, *J. Am. Chem. Soc.*, 2024, **146**, 29575–29587.
80 A. Singh and M. I. S. Röhr, *J. Chem. Theory Comput.*, 2024, **20**, 8624–8633.
81 M. T. Trinh, Y. Zhong, Q. Chen, T. Schiros, S. Jockusch, M. Y. Sfeir, M. Steigerwald, C. Nuckolls and X. Zhu, *J. Phys. Chem. C*, 2015, **119**, 1312–1319.
82 M. Chen, N. E. Powers-Riggs, A. F. Coleman, R. M. Young and M. R. Wasielewski, *J. Phys. Chem. C*, 2020, **124**, 2791–2798.
83 M. Chen, A. F. Coleman, R. M. Young and M. R. Wasielewski, *J. Phys. Chem. C*, 2021, **125**, 6999–7009.
84 G. He, K. R. Parenti, L. M. Campos and M. Y. Sfeir, *Adv. Mater.*, 2022, **34**, 2203974.
85 S. Nakamura, H. Sakai, M. Fuki, Y. Kobori, N. V. Tkachenko and T. Hasobe, *J. Phys. Chem. Lett.*, 2021, **12**, 6457–6463.
86 S. Nakamura, H. Sakai, M. Fuki, R. Ooie, F. Ishiwari, A. Saeki, N. V. Tkachenko, Y. Kobori and T. Hasobe, *Angew. Chem., Int. Ed.*, 2023, **62**, e202217704.
87 A. B. Kolomeisky, X. Feng and A. I. Krylov, *J. Phys. Chem. C*, 2014, **118**, 5188–5195.
88 T. Kakitani, A. Kimura and H. Sumi, *J. Phys. Chem. B*, 1999, **103**, 3720–3726.
89 A. Kimura and T. Kakitani, *J. Phys. Chem. B*, 2003, **107**, 14486–14499.
90 A. Kimura and T. Kakitani, *J. Phys. Chem. A*, 2007, **111**, 12042–12048.
91 A. Kimura, T. Kakitani and T. Yamato, *J. Phys. Chem. B*, 2000, **104**, 9276–9287.
92 A. Kimura, T. Kakitani and T. Yamato, *Int. J. Mod. Phys. B*, 2001, **15**, 3833–3836.
93 G. D. Scholes, *J. Phys. Chem.*, 1996, **100**, 18731–18739.
94 Y. Kobori, T. Yago, K. Akiyama, S. Tero-Kubota, H. Sato, F. Hirata and J. R. Norris, *J. Phys. Chem. B*, 2004, **108**, 10226–10240.
95 M. B. Zimmt and D. H. Waldeck, *J. Phys. Chem. A*, 2003, **107**, 3580–3597.
96 A. S. Lukas, P. J. Bushard and M. R. Wasielewski, *J. Phys. Chem. A*, 2002, **106**, 2074–2082.
97 J. Z. Low, S. N. Sanders and L. M. Campos, *Chem. Mater.*, 2015, **27**, 5453–5463.
98 D. O. Balakirev, Y. N. Luponosov, A. L. Mannanov, S. A. Pisarev, D. Y. Paraschuk and S. A. Ponomarenko, *J. Photonics Energy*, 2018, **8**, 044002.
99 J. Yi, G. Zhang, H. Yu and H. Yan, *Nat. Rev. Mater.*, 2024, **9**, 46–62.